International Journal of Chemical, Materials and Biomolecular Sciences
ISSN: 2415-6620
Vol:13, No:11, 2019

Electrochemical Response Transductions of Graphenated-Polyaniline Nanosensor for Environmental Anthracene

O. Tovide, N. Jahed, N. Mohammed, C. E. Sunday, H. R. Makelane, R. F. Ajayi, K. M. Molapo, A. Tsegaye, M. Masikini, S. Mailu, A. Baleg, T. Waryo, P. G. Baker, E. I. Iwuoha

***Abstract*—**A graphenated–polyaniline (GR-PANI) nanocomposite sensor was constructed and used for the determination of anthracene. The direct electro-oxidation behavior of anthracene on the GR-PANI modified glassy carbon electrode (GCE) was used as the sensing principle. The results indicate thatthe response profile of the oxidation of anthracene on GR-PANI-modified GCE provides for the construction of sensor systems based onamperometric and potentiometric signal transductions. A dynamic linear range of 0.12-100 μM anthracene and a detection limit of 0.044 μM anthracene were established for the sensor system.

***Keywords*—**Electrochemical sensors, environmental pollutants, graphenated-polymers, polyaromatic hydrocarbon.

I. Introduction

THE growing concern about the environment and human health has resulted in the search for effective methodsfor detecting and analysing environmental contaminants. Polyaromatic hydrocarbons (PAHs) are among the persistent organic pollutants (POPs) that have deleterious health effects on both aquatic organisms and humans [1], [2]. PAHs are a class of chemical compounds that have more than one fused aromatic rings. They are products of incomplete combustion of petroleum, coal, tar and other forms of organic materials [3]. Anthracene, phenanthrene, fluoranthene, benz[a]anthracene and benz[a]pyrene are some examples of PAHs [4] that have been detected at all levels of the food chain [5]. Consequently, the European Union, World Health Organization (WHO) and several countries have regulations for PAHs in food and environment [6], [7].

Sensors are necessary for real time checking of adherence to the set limits of PAHs. Intrinsically conducting polymers (ICPs) and their composites are known to be very effective materials for the construction of sensors [8]. In particular, graphene-based polymeric nanomaterials are expected to possess properties that make them very efficient platforms for the development of electrochemical sensors [9]. Due to the excellent electronics of its two-dimensional sp^2-hybridized carbons, electrocatalys is readily occurs on graphene film [10], [11]. This property of graphene can be modified by the incorporation of functional nanomaterials to produce required electrochemical sensing performance [12]. Doped form of ICPs, such as polyaniline (PANI), have been recognized as cost effective electrocatalytic sensor materials due to their improved redox activity and conductivity [13], [14].

Doped PANI has been reported [15], [16] to be characterised by enhanced mechanical, electrical, thermal and elctrochemical properties [17]. In the form of nanosheets graphene can provide active nucleation sites for PANI as well as excellent electron transfer pathways [18]. GR-PANI nanocomposite-based sensor for anthracene is being presented for the first time in this report.

O. Tovide, N. Jahed, N. Mohammed, C. E. Sunday, H. R. Makelane, R. F. Ajayi, K. M. Molapo, A. Tsegaye, M. Masikini, Stephen Mailu, A. Baleg, T. Waryo, P. G. Baker, and E. I. Iwuoha are with SensorLab, University of the Western Cape, Bellville, Cape Town, 7535, South Africa (phone: 27 21 9593054; fax: 27 21 959 3055; e-mail: eiwuoha@uwc.ac.za).

II. Experimental

A. Reagents

Natural graphite powder (microcrystal grade, 99.9995%) (Metal base) UCP1-M grade, Ultra "F" purity was purchased from Alfa Aesar and used for the preparation of graphene oxide (GO) by a modified Hummers method [19]. Analytical grade aniline (99%) was obtained from Aldrich Chemical, Gillingham, England and purified by distillation under reduced pressure prior to use. Ammonium persulphate ($(NH_4)_2S_2O_8$), anthracene (99%), lithium perchlorate ($LiClO_4$, 99.99%), acetonitrile (HPLC grade), hydrochloric acid (HCl, 37%), hydrogen peroxide (H_2O_2, 35 wt % water solution), sulphuric acid (H_2SO_4), sodium nitrite ($NaNO_2$) and potassium permanganate ($KMnO_4$) were obtained from Sigma-Aldrich. 0.1M $LiClO_4$ in acetonitrile was used as the supporting electrolyte. Ultra-pure water (Millipore) was used for all preparations.

B. Apparatus

Cyclic voltammetry (CV) and square wave voltammetry (SWV) were performed with a BAS 100W electrochemical workstation from BioAnalytical Systems (BAS) Technicol Ltd., Stockport, UK. A conventional three-electrode system was used and it consisted of a GCE, Ag/AgCl (with 3 M NaCl saltbridge) and platinum wire as the working, reference and counter electrodes, respectively. The infrared spectra of PANI, graphite, graphite oxide and graphene were recorded on a Fourier Transform Infra-Red (FTIR) spectrometer (Perkin Elmer Spectrum 100) and their structural details were evaluated by X-ray diffraction studies performed with a Phillips X-ray diffractometer that has Cu-Kα radiation. A

tapping-mode atomic force microscope (Veeco Nanoman V) was used to evaluate the morphology of graphene and its film thickness. An-doped (antimony) silicon tip (with a curvature radius of 2.5 - 3.5 μm, a force constant of 1 - 5N $m^{-1}$and a resonance frequency of 60 - 100 kHz) was used for the atomic force microscopy (AFM) esperiments. The samples for AFM were prepared by drop-coating a silicon wafer with 5μL graphene/water dispersion. Transmission electron microscopy (TEM) images of materials were obtained with a Tecnai G_2 F20X-Twin MAT 200KV high resolution (HR) TEM from FEI (Eindhoven, Netherlands). Scanning electron microscopy (SEM) were performed with a LEO 1450 SEM 3OKV instrument equipped with energy dispersive X-ray (EDX) and wavelength-dispersive spectrometry (WDS) capabilities. Electrochemical impedance spectroscopy (EIS) measurements were performed on VoltaLab PGL 402 from Radiometer Analytical (Lyon, France) in 1 M HCl.

C. Material Synthesis

GO was synthesized from graphite powder by the modified Hummers method [19]. 2.0 g powdered graphite flake sand 1.0 g $NaNO_2$ were gently added to 50mL concentrated H_2SO_4 at room temperature. The solution was then cooled to 0 °C in an ice bath while stirring vigorously. 7.0 g $KMnO_4$ was added to the suspension and the rate of addition was carefully controlled to prevent the temperature of the suspension from exceeding 20 °C. The ice bath was then removed and the temperature of the suspension was raised to room temperature and maintained for 30 min. The temperature was then raised to 35 °C in a water bath and then stirred for 2 h. As the reaction progressed, the slurry gradually thickened with diminishing effervescence. The mixture was cooled in ice bath and excess deionised water was added to it. The reaction mixture was treated with 35% H_2O_2 until gas evolution ceased, in order to reduce the residual $KMnO_4$ and MnO_2 to colourless and soluble $MnSO_4$. The precipitate was filtered off, washed several times with warm deionized water/concentrated HCI mixed solvent (9/1 volume ratio) and then dried under reduced pressure at 60 °C for 24h to obtain GO. The GO was then exfoliated in distilled water through ultrasonication to form thin GO sheets for subsequent use.

GR-PANI was prepared by *in situ* polymerization of aniline in a suspension of GO, by chemical oxidation of aniline with $(NH_4)_2S_2O_8$ in an acidic medium [17], followed by the reduction of the solution with $NaBH_4$ [20]. The reaction product was then dispersed in1 M HCl containing $(NH_4)_2S_2O_8$ and stirred overnight at room temperature to allow the reoxidation and reprotonation of PANI to occur and form crystalline GR-PANI. The resultant GR-PANI nanocomposite was collected by filtration and dried in vacuum. For comparison, PANI film was prepared by the same procedure under the same condition but without adding GO. Graphene nanosheets were also synthesized and by $NaBH_4$ reduction. Typically 100 mg GO powder was dispersed in 100mL deionised water and exfoliated into GO sheets by ultrasonication for 1 h to form a stable aqueous dispersion. 200 mg $NaBH_4$ was then added to the dispersion while stirring the mixture continuously at 125 °C for 3 h. Finally a black precipitate was obtained and isolated by filtration and dried under vacuum at 60 °C to obtain graphene [20].

D. Preparation of Modified Electrodes

A 0.071 cm^2 GCE was polished with slurries of 0.05, 0.3 and 1.0 μm alumina powder (Buehler, IL, USA), rinsed with distilled water, ultrasonicated in ethanol and deionised water, and then dried at room temperature. 1 mg GR-PANI nanocomposite was dispersed in 1 mL ethanol and ultrasonicated for 30 min to form a homogenous suspension. The surface of a GCE was coated with 5 μL of the suspension and dried at room temperature to form GR-PANI|GCE sensor. PANI|GCE and GR|GCE systems were also prepared by drop-coating GCE with 5 μL of their respective suspensions.

III. Results and Discussion

A. Characterization of GR-PANI Nanocomposite

The CV of GR-PANI|GCE was run in 1M HCl within a potential window of -0.2 to +1.2 V vs. Ag/AgCl. The electrochemical reactivities of the different electrodes are depicted in the CVs presented in Figs. 1 (a)-(d). As shown by the innermost voltamogram (unlabled) in Fig. 1 (a), no peak was observed for unmodified GCE, but after modification with graphene, i.e. CVs (i - v), a pair of redox peaks was observed. The peaks increased as scan rate increased, accompanied by an anodic and cathodic shifts in oxidation and reduction peak potentials, respectively. This behavior is typical of carbon materials because of the transition between quinone and hydroquinone electrochemistry [15]. The PANI|GCE system depicted in Fig. 1 (b) has two redox couples labeled $I_{p.c1}/I_{p.c\ 1}$ and $I_{p.a\ 2}/I_{p.c\ 2}$, as is typical with PANI redox transitions of the semiconductive leucomeraldine form ($I_{p.c\ 1}$) to the conductive polaronic-leucomeraldine form ($I_{p.a\ 1)}$); and the faradaic transformation of emeraldine ($I_{p.c\ 2}$) to penigraniline ($I_{p.a\ 2}$) [21]. The CV of GR-PANI-modified GCEis characterized by well-defined redox peaks and an enhancement of the peak currents relative to those of PANI-modified and unmodified GCE. The current density and the anodic to cathodic peak separation (ΔE_p) analyses of the CVs drawn in Fig. 1 (b) gave $\Delta E_{p(1)}$ and $\Delta E_{p(2)}$ values of 184 and 137 mV, respectively, for PANI|GCE. The corresponding values for GR-PANI|GCE were 83 and 51 mV. The results demonstrate a graphene-induced reduction in the ΔE_p values of PANI by a factor of 2.2 for the leucomeraldine/polaronic-leucomeraldine transition, and 2.7 for the emeraldine/penigraniline process. The reduction in the ΔE_p value means that the electrochemistry of the graphenated system is faster and the material is more conducting.

In addition to the good conductivity of graphene, its excellent catalytic properties as a result of its higher surface-to-volume ratio, provides greater surface accessibility of the polymer matrix [22], [23].

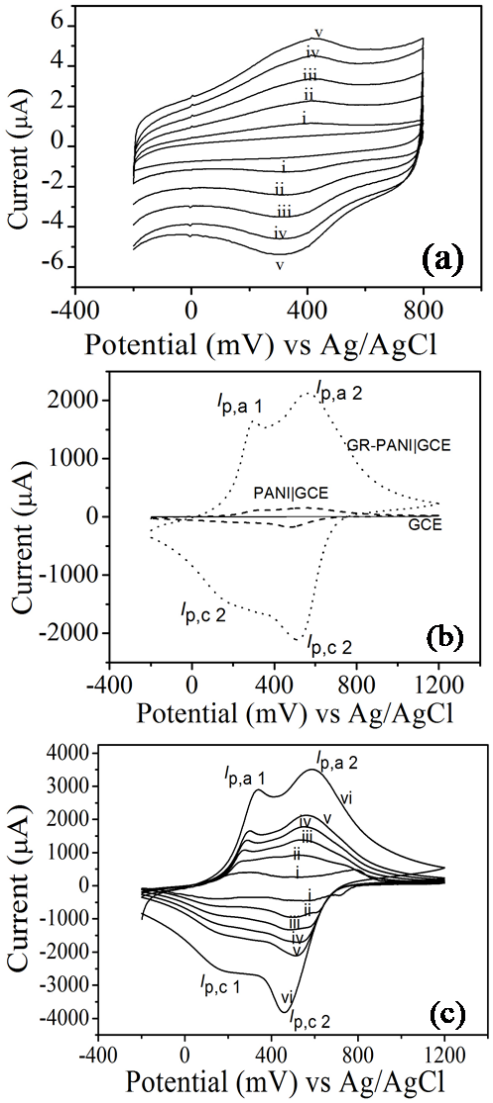

Fig. 1 Cyclic voltammograms of (a) GCE (innermost CV) and GR|GCE at scan rates of (i)10,(ii) 20, (iii) 30, (iv) 40 and (v) 50 mV s^{-1}; (b) GCE, PANI|GCE and GR-PANI|GCE at 50 mV s^{-1} in 1 M HCl(b); and (c) GR-PANI|GCE in 1 M HCl at scan rates of (i) 10, (ii) 20, (iii) 30 (iv) 40 (v) 50 and (vi) 100 mV s^{-1}

The anodic peak currents ($I_{p,a1}$ and $I_{p,a\ 2}$) of GR-PANI|GCE (Fig. 1 (c)) were found to be linearly dependent on scan rates, in accordance with the equations: $I_{p,a\ 1} = 2.0461\times 10^{-4} + 2.7413 \times 10^{-5}\,x(r^2 = 0.9980)$; $I_{p,a2} = 3.0782 \times 10^{-4} + 3.3360 \times 10^{-5}x$ ($r^2 = 0.9930$). This behavior is in agreement with that of a thin film of adsorbed electroactive species undergoing a Nernstian reaction [24], [25].The surface concentration, Γ^* (mol cm^{-2}), of the adsorbed electroactive species can be estimated from (1):

$$\frac{I_{p,a}}{\nu} = \frac{n^2F^2A\Gamma^*_{GR\text{-}PANI}}{4RT} \quad (1)$$

where n is the number of electron transferred, F is Faraday constant (96500 C mol^{-1}), $\Gamma^*_{GR\text{-}PANI}$ is surface concentration of GR-PANI film(mol cm^{-2}), A is surface area of GCE (0.071 cm^2), ν is scan rate (mV s^{-1}), R is gas constant (8.314 $Jmol^{-1}K^{-1}$) and T is temperature (298 K). The evaluation of n from the slope of the linear $I_{p,a\ 1}$ vs. ν plot predicted a one electron process for the leucoemeraldine/polaronic-leucomeraldine transition, as reported by other workers [26], [27]. The $\Gamma^*_{GR\text{-}PANI}$ value was evaluated to be 3.073×10^{-9} mol cm^{-2}.

B. EIS of GR-PANI|GCE

Electrochemical impedance spectroscopy was used to investigate the conductivity of the modified electrodes [28]-[30]. The measurement was performed in 1M HCl at a frequency range of 100 kHz to 0.1 Hz and an alternate voltage of 10 mV. The Nyquist plots of the EIS results are in Fig. 3. The plots displayed significant differences in the diameter of the Nyquist semicircles upon the modification of the electrodes. The charge transfer resistance (R_{ct}) values calculated after fitting the EIS data to the Randle's equivalent circuit diagram in Fig. 2 (inset) are 51.2,27.68 and 20.32 kΩ for GCE, PANI|GCE, GR-PANI|GCE, respectively. The values confirm that graphene decreased the resistance of PANI by 7 kΩ suggesting the suitability of GR-PANI as a good conducting platform for electrocatalysis.

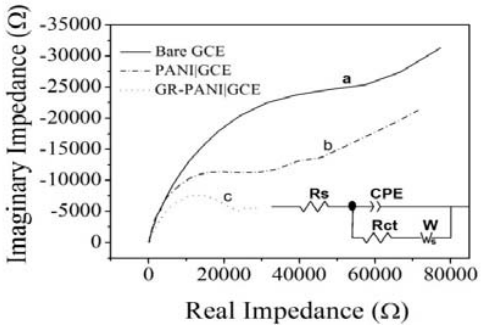

Fig. 2 Nyquist plots of the EIS data of (a) GCE, (b) PANI|GCE and (c) GR-PANI|GCE in 1 M HCl. Inset is the Randle's equivalent circuit used for fitting the Nyquist plots

C. Surface Morphology and Structure

The SEM images of the GR-PANI sensor components are displayed in Fig. 3. The exfoliated GO sheets (Fig. 3 (a)) closely resemble the disordered and crumbled sheet of graphene (Fig. 3 (b)). The GR-PANI (Fig. 3 (c)) exhibits fibrous PANI moieties that are intercalated between graphene sheets, in contrast to the porous fibrillar structure of PANI film in Fig. 3 (d).

HRTEM images presented in Fig. 4 are those of (a) GO, (b) graphene, (c) PANI and (d) GR-PANI. The GO image resembles layers of sheets that are folded in places. Flat transparent thin layer sheets can be observed for graphene. In the inset of Fig. 4 (b), the selected area electron diffraction (SAED) pattern confirmed the crystallinity of the material. The HRTEM of PANI in Fig. 4 (c) reveals a uniform fibrous material while the GR-PANI nanocomposite depicts

homogeneously distributed nanotubes. The nanotubes seem to be PANI formations on templates created by the graphene sheets.

Fig. 5 is the FTIR spectra of GR-PANI as well as the reagents used in its preparation. GO spectrum (d) has absorption bands corresponding to the following functional groups: C=O (1735 cm^{-1}), aromatic C=O (1602 cm^{-1}), carboxyl C-O (1416 cm^{-1}), epoxy C-O (1265 cm^{-1}), alkoxy C-O (1047 cm^{-1}) and hydroxyl O-H (3390 cm^{-1}).

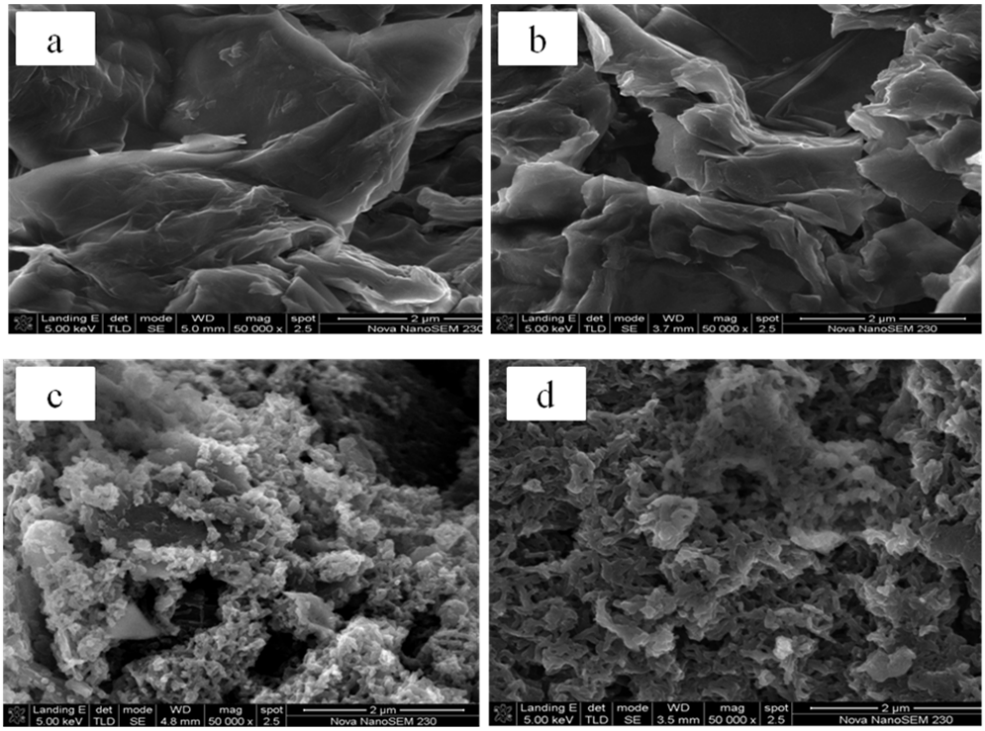

Fig. 3 SEM images of (a) GO, (b) GR, (c) GR-PANI and (d) PANI

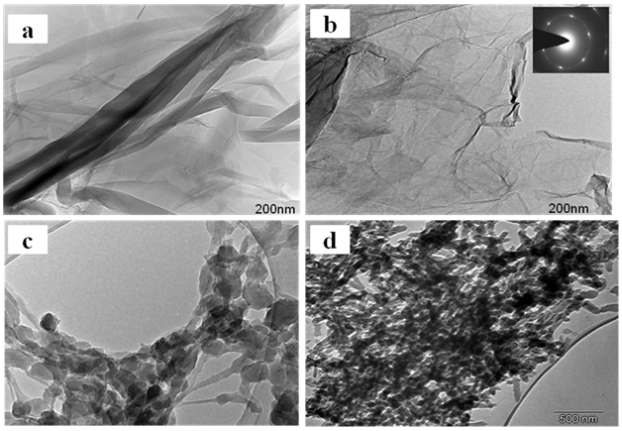

Fig. 4 HRTEM pictures of (a) GO, (b) GR, (c) PANI and (d) GR-PANI

The FTIR results for GO are in agreement with previous spectra reported in other studies [31]. However, the intensity of the absorption band of GO at 1735 cm^{-1} (C=O) decreased after the formation of graphene sheets by the reduction of GO. The characteristic absorption bands of emaraldine PANI were observed in the FTIR of PANI (spectrum c), including the band at 1568 and 1476 cm^{-1} that can be assigned to the stretching vibration of quinone and benzene rings, respectively. The bands at 1290 and 1233 cm^{-1} correspond to the C-N stretching vibration. The in-plane bending and out-of-plane bending of C-H stretching of PANI are manifested by the bands at 1111 and 791 cm^{-1}, respectively [32]. The FTIR spectrum of GR-PANI (b) revealed the interactions between graphene and PANI which results in the decrease or disappearance of the characteristic bands of PANI at 1250, 1400 and 1600 cm^{-1}.

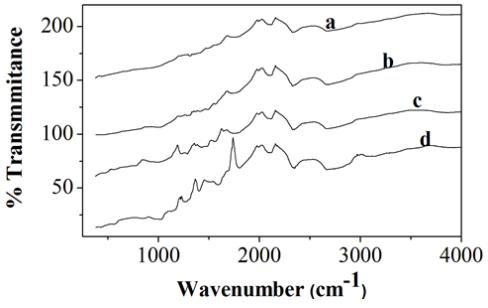

Fig. 5 FTIR spectra of (a) GR, (b) GR-PANI, (c) PANI and (d) GO

The AFM topographical image of grapheme (Fig. 6) can be interpreted to indicate randomly assembled graphene sheets on

a silicon substrate. The graphene surface was slightly rough and this could be due to the existence of some defects from functional groups. Analysis of the cross sectional view along the plain area of the sheet gave an estimated film height of 1.4 nm, which is consistent with what was reported by Willemse et al. [33]. The XRD patterns of GR (a), PANI (b) and GR-PANI composites (c) are presented in Fig. 7. GR showed broad diffraction peaks at 24.2° (002) and 43.6° (100) with some crystalline features of graphite-like structures. The broadening of the peak can be attributed to the loosely stacked sheets in graphene [34]. PANI revealed a slightly broadened peak at ~ 25.4° and another low intensity peak at 12.7° which are the peaks of the crystal planes of PANI in its emeraldine salt form [17]. The GR-PANI nanocomposite has XRD patterns that are similar to the merging of those of graphene and PANI [23]. This is consistent with the conclusions drawn from the SEM and TEM studies.

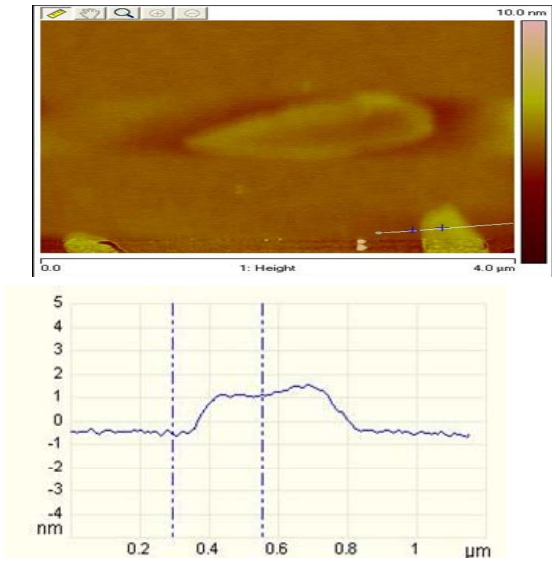

Fig. 6 AFM image of graphene sheets on silicon substrate and the plot of the cross sectional height profile

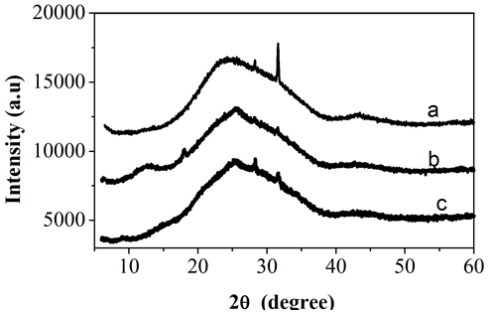

Fig. 7 XRD patterns of (a) GR, (b) PANI and (c) GR-PANI

D. Anthracene Sensor

The response of GR-PANI|GCE sensor to anthracene was studied in acetonitrile/water containing 0.1 M $LiClO_4$ as the supporting electrolyte. An anodic peak at +1101 mV with no reduction peak was ascribed to the oxidation of anthracene on the GR-PANI electrode. Anthraquinone is suggested to be rapidly formed as a result of the irreversible oxidation process [35]. The oxidation of PAHs by electrochemical degradation is usually initiated by direct electron transfer from adsorbed PAH to the electrode, which generates cationic radicals that undergo subsequent reactions [36], [37]. The oxidation of anthracene in acetonitrile-containing small amount of water is a one-electron reaction, that appears to be the initial step [38] that is followed by the formation of radical cations and then 9,10-anthraquinone as the final product [36], [37]. However, it is important to note that a small amount of water in acetonitrile plays a crucial role in the oxidation of anthracene by actually favoring the production of the final product [38]. A possible mechanism for the oxidation of anthracene to anthraquinone is presented in Fig. 8.

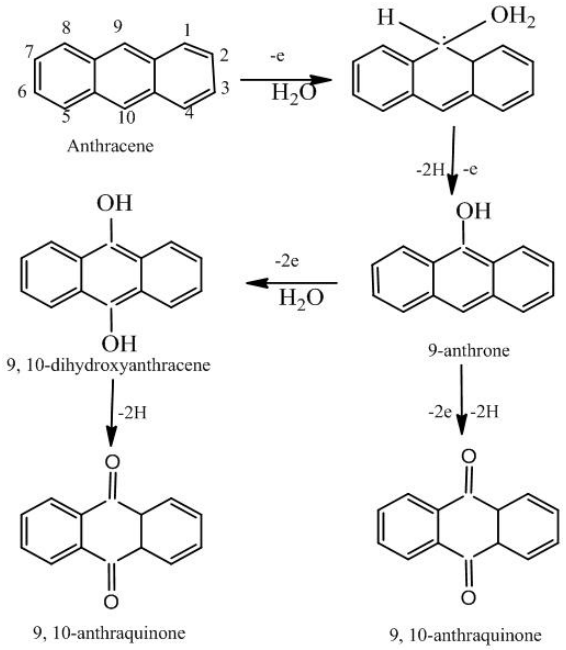

Fig. 8 Mechanism for the oxidation of anthracene

The electrochemical oxidation of 100µM anthracene on PANI|GCE, GR-PANI|GCE and unmodified GCE in acetonitrile/water (80:20 v/v) containing 0.1M $LiClO_4$ as the supporting electrolyte, was studied by CV and the results are plotted in Fig. 9. In the absence of anthracene the electrode systems ('a' and 'b') exhibited electroactivity between 1 and 800 mV. However, in the presence of 100µM anthracene, irreversible electro-oxidation reactions of anthracene occur on the PANI|GCE (c) and GR-PANI|GCE (d) electrode systems. The reactions are characterized by the formation of anodic peaks at approximately +1101 mV [35]. The electrocatalytic current produced by 100µM anthracene was higher for GR-PANI|GCE than PANI|GCE, thereby confirming that graphene enhanced the electrocatalytic reaction. No catalysis of anthracene was observed on unmodified GCE. The analysis of the scan rate dependence of the anthracene oxidation current on GR-PANI|GCE (presented in the CVs of Fig. 10) gave a

Randel Sevčik relationship, which indicated that the process was limited by the rate of diffusion of anthracene from the solution to surface of the electrode [39], [40].

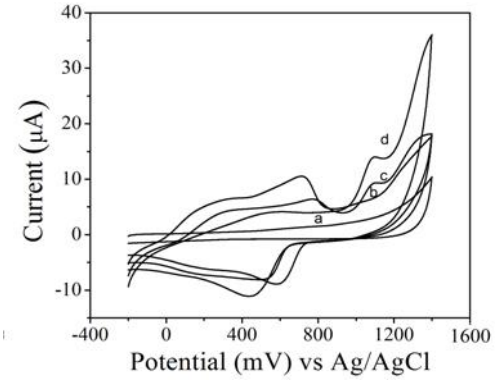

Fig. 9 CVs of (a) GCE and (b) GR-PANI|GCE in 0 μM anthracene; (c) PANI|GCE and (d) GR-PANI|GCE in 100 μM anthracene. Experimental conditions: 0.1 M $LiClO_4$in acetonitrile/water (80:20 v/v) and scan rate of 50 mV s^{-1}

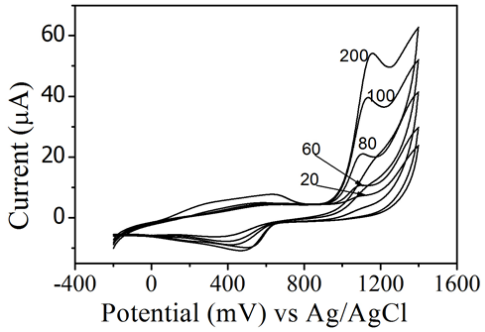

Fig. 10 Scan rate dependence of the CV responses of GR-PANI|GCE sensor to 100 μM anthracene. Experimental conditions: 0.1 M $LiClO_4$ in acetonitrile/water (80:20 v/v). Numbers on the plots are scan rates in mV s^{-1}

It is noteworthy that the oxidation peak potentials at 1101 mV shifted anodically with increase in scan rate, as is characteristic of irreversible electrocatalytic process[39].

The CV responses of GR-PANI|GCE sensor are plotted in Figs. 11 (a) and (b) for low and high concentrations of anthracene, respectively. Fig. 12 presents the SWV responses of the sensor for 20-1000 μM anthracene. The anthracene sensor (GR-PANI|GCE) was calibrated with CV and SWV peak current values obtained from Figs. 11 and 12. The CV and SWV peak currents exhibited a linearrelationship with anthracene concentration up to 100μM anthracene. This region represents the dynamic linear range (DLR) for the application of the sensor for anthracene determination. The DLR value for the GR-PANI|GCE senor system was 0.12-100 μM anthracene and the associated limit of detection (LOD) was 0.044μM anthracene. The value of the DLR depends on the physical properties of the sensor including the amount of the sensor material (GR-PANI) on the electrode.

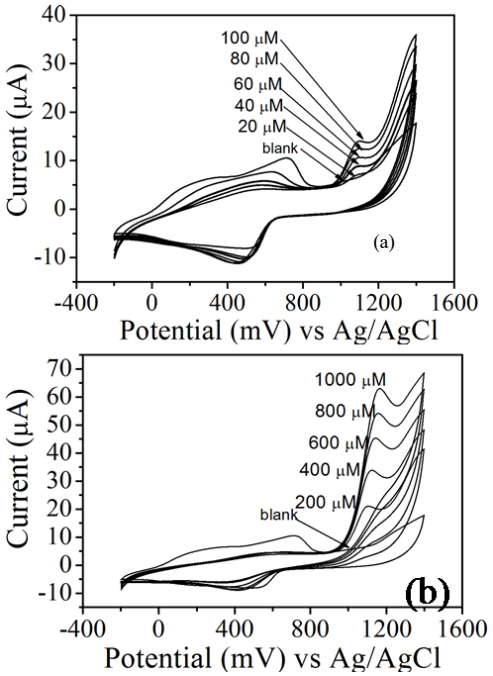

Fig. 11 CV responses of GR-PANI|GCE sensor to anthracene at 50 mV s^{-1}.Experimental conditions: 0.1 M $LiClO_4$ in acetonitrile/water (80:20 v/v) for (a) 20-100 μM and (b) 200-1000 μM anthracene

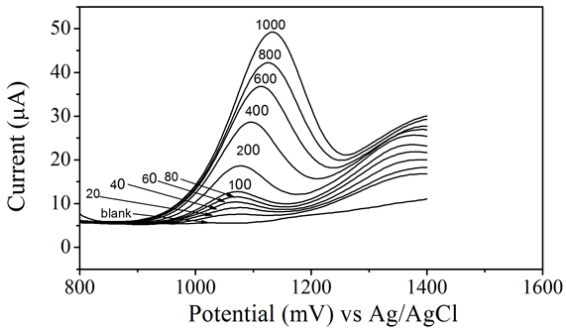

Fig. 12 SWV responses of GR-PANI|GCE sensor to 20 - 1000μM anthracene. Experimental conditions: 0.1 M $LiClO_4$ in acetonitrile/water (80:20 v/v). (SW frequency = 5 Hz and SW amplitude = 25mV)

E. Reproducibility, Stability and Interference Studies

Stability and reproducibility studies were performed by the analysis of 3 successive measurements (n=3) of the CV responses of GR-PANI|GCE sensor to 100μM anthracene. A relative standard deviation of 1.5% was obtained, which indicates excellent reproducibility of the CV measurements. The sensor response was also measured for a period of 3 weeks during which measurements were made at 4-day intervals in order to ascertain the storage stability of the sensor. The GR-PANI|GCE sensor system was stored in the refrigerator at 4 °C in between measurements. During the 3-week storage period, the sensor retained 89% of the magnitude of its original signal.

$Mn^{2+,}$ Cl^{-}, $SO4^{2-}$ and NO^{3-} ions did not exhibit any

intereference with the detection of 100 µM anthracene.

IV. Conclusion

The GR-PANI|GCE electrochemical sensor exhibited excellent amperometric signal tranduction for the determination of anthracene. The sensor's LOD value of 0.044 µM is similar to the LOD values reported for other types of anthracene sensors [39]. That notwithstanding, this study has introduced a new class of electroactive platform (graphenated electractive polymers) for the development of electrochemical sensor systems. Also the wide dynamic linear range of the electrode offers the possibility of the application of this type of sensor system to sample matrices with a wide range of analyte concentrations. The peak potentials of the square wave voltammetric determination of anthracene (Fig. 12) shifted from +1110 mV for 20 µM anthracene to +1125mV for 1000 µM anthracene. This predicts that the sensor can be calibrated potentiometrically in addition to the amperometric signal transduction reported in this study.

References

[1] V. Vestreng, H. Klein, Emission data reported to UNECE/EMEP: Quality assurance and trend analysis and presentation of WebDab, *MSC-W Status Report*, 2002.

[2] S. Xu, W. Liu, S. Tao, Emission of polycyclic aromatic hydrocarbons in China,*Environ. Sci. Technol*, vol. 40, pp. 702-708, 2006.

[3] A. Mastral, T. García, M. Callén, M. Navarro, J. Galbán, Removal of naphthalene, phenanthrene and pyrene by sorbents from hot gas, *Environ. Sci. Technol*, vol. 35, pp. 2395-2400, 2001.

[4] J. C. Fetzer, *Large (C= 24) Polycyclic Aromatic Hydrocarbons:* Wiley-Interscience: New York 2000.

[5] P. Plaza-Bolaños, A. G. Frenich, J. L. M. Vidal, Polycyclic aromatic hydrocarbons in food and beverages. Analytical methods and trends, *J. Chromatogr. A*, vol. 1217, pp. 6303-6326, 2010.

[6] C.-E. Boström, P. Gerde, A. Hanberg, B. Jernström, C. Johansson, T. Kyrklund, A. Rannug, M. Törnqvist, K. Victorin, R. Westerholm, Cancer risk assessment, indicators, and guidelines for polycyclic aromatic hydrocarbons in the ambient air, *Environ. Health Perspect.*, vol. 110, pp. 451-488, 2002.

[7] R. E. Bain, S. W. Gundry, J. A. Wright, H. Yang, S. Pedley, J. K. Bartram, Accounting for water quality in monitoring access to safe drinking-water as part of the millennium development goals: lessons from five countries, *Bull. WHO*, vol. 90, pp. 228-235, 2012.

[8] S. Bhadra, D. Khastgir, N. K. Singha, J. H. Lee, Progress in preparation, processing and applications of polyaniline, *Prog. Polym. Sci*, vol. 34, pp. 783-810, 2009.

[9] M. Pumera, R. Scipioni, H. Iwai, T. Ohno, Y. Miyahara, M. Boero, A mechanism of adsorption of β-nicotinamide adenine dinucleotide on graphene sheets: Experiment and theory, *Chem. Eur. J.*, vol. 15, pp. 10851-10856, 2009.

[10] L. Tang, Y. Wang, Y. Li, H. Feng, J. Lu, J. Li, Preparation, structure, and electrochemical properties of reduced graphene sheet films, *Adv. Funct. Mater.*, vol. 19, pp. 2782-2789, 2009.

[11] A. K. Geim, K. S. Novoselov, The rise of graphene, *Nature Mater.*, vol. 6, pp. 183-191, 2007.

[12] C. Shan, H. Yang, D. Han, Q. Zhang, A. Ivaska, L. Niu, Graphene/AuNPs/chitosan nanocomposites film for glucose biosensing,*Biosens. Bioelectron*., vol. 25, pp. 1070-1074, 2010.

[13] D. S. Patil, J. Shaikh, S. Pawar, R. Devan, Y. Ma, A. Moholkar, J. Kim, R. Kalubarme, C. Park, P. Patil, Investigations on silver/polyaniline electrodes for electrochemical supercapacitors, *Phys. Chem. Chem. Phys.*, vol. 14, pp. 11886-11895, 2012.

[14] S. Virji, J. Huang, R. B. Kaner, B. H. Weiller, Polyaniline nanofiber gas sensors: examination of response mechanisms, *Nano Lett.*, vol. 4, pp. 491-496, 2004.

[15] D.-W. Wang, F. Li, J. Zhao, W. Ren, Z.-G. Chen, J. Tan, Z.-S. Wu, I. Gentle, G. Q. Lu, H.-M. Cheng, Fabrication of graphene/polyaniline composite paper via *in situ* anodic electropolymerization for high-performance flexible electrode, *ACS Nano*, vol. 3, pp. 1745-1752, 2009.

[16] K. Zhang, L. L. Zhang, X. Zhao, J. Wu, Graphene/polyaniline nanofiber composites as supercapacitor electrodes, *Chem.Mater*., vol. 22, pp. 1392-1401, 2010.

[17] J. Yan, T. Wei, B. Shao, Z. Fan, W. Qian, M. Zhang, F. Wei, Preparation of a graphene nanosheet/polyaniline composite with high specific capacitance, *Carbon*, vol. 48, pp. 487-493, 2010.

[18] C. Vallés, P. Jiménez, E. Muñoz, A. M. Benito, W. K. Maser, Simultaneous reduction of graphene oxide and polyaniline: doping-assisted formation of a solid-state charge-transfer complex, *J. Phys. Chem. C*, vol. 115, pp. 10468-10474, 2011.

[19] D. Li, M. B. Mueller, S. Gilje, R. B. Kaner, G. G. Wallace, Processable aqueous dispersions of graphene nanosheets, *Nat. Nanotechnol.*, vol. 3, pp. 101-105, 2008.

[20] H. J. Shin, K. K. Kim, A. Benayad, S. M. Yoon, H. K. Park, I. S. Jung, M. H. Jin, H. K. Jeong, J. M. Kim, J. Y. Choi, Efficient reduction of graphite oxide by sodium borohydride and its effect on electrical conductance, *Adv. Funct. Mater*., vol. 19, pp. 1987-1992, 2009.

[21] Y. G. Wang, H. Q. Li, Y. Y. Xia, Ordered whisker-like polyaniline grown on the surface of mesoporous carbon and its electrochemical capacitance performance, *Adv. Mater.*, vol. 18, pp. 2619-2623, 2006.

[22] S. Stankovich, D. A. Dikin, R. D. Piner, K. A. Kohlhaas, A. Kleinhammes, Y. Jia, Y. Wu, S. T. Nguyen, R. S. Ruoff, Synthesis of graphene-based nanosheets via chemical reduction of exfoliated graphite oxide, *Carbon*, vol. 45, pp. 1558-1565, 2007.

[23] G. Wang, S. Zhuo, W. Xing, Graphene/polyaniline nanocomposite as counter electrode of dye-sensitized solar cells, *Adv. Mater*., vol. 69, pp. 27-29, 2012.

[24] A. A. Shah, R. Holze, Spectroelectrochemistry of two-layered composites of polyaniline and poly(o-aminophenol), *Electrochim. Acta*, vol. 53, pp. 4642-4653, 2008.

[25] E. I. Iwuoha, D. Saenz de Villaverde, N. P. Garcia, M. R. Smyth, J. M. Pingarron, Reactivities of organic phase biosensors. 2. The amperometric behavior of horseradish peroxidase immobilised on a platinum electrode modified with an electrosynthetic polyaniline film, *Biosens. Bioelectron.*, vol. 12, pp. 749-761, 1997.

[26] A. J. Bard, L. R. Faulkner, *Electrochemical methods: fundamentals and applications*. Wiley New York, 1980.

[27] E. I. Iwuoha, S. E. Mavundla, V. S. Somerset, L. F. Petrik, M. J. Klink, M. Sekota, P. Bakers, Electrochemical and spectroscopic properties of fly ash–polyaniline matrix nanorod composites, *Microchim. Acta*, vol. 155, pp. 453-458, 2006.

[28] R. Ehret, W. Baumann, M. Brischwein, A. Schwinde, K. Stegbauer, B. Wolf, Monitoring of cellular behavior by impedance measurements on interdigitated electrode structures, *Biosens. Bioelectron*., vol. 12, pp. 29-41, 1997.

[29] X. Kang, Z. Mai, X. Zou, P. Cai, J. Mo, A novel glucose biosensor based on immobilization of glucose oxidase in chitosan on a glassy carbon electrode modified with gold–platinum alloy nanoparticles/multiwall carbon nanotubes, *Anal. Biochem.*, vol. 369, pp. 71-79, 2007.

[30] L. Wang, E. Wang, Direct electron transfer between cytochrome c and a gold nanoparticles modified electrode, *Electrochem. Commun.*, vol. 6, pp. 49-54, 2004.

[31] W. Chen, L. Yan, P. R. Bangal, Preparation of graphene by the rapid and mild thermal reduction of graphene oxide induced by microwaves, *Carbon*, vol. 48, pp. 1146-1152, 2010.

[32] J. Yin, X. Zhao, X. Xia, L. Xiang, Y. Qiao, Electrorheological fluids based on nano-fibrous polyaniline, *Polym. J.*, vol. 49, pp. 4413-4419, 2008.

[33] C. M. Willemse, K. Tlhomelang, N. Jahed, P. G. Baker, E. I. Iwuoha, Metallo-graphene nanocomposite electrocatalytic platform for the determination of toxic metal ions, *Sensors*, vol. 11, pp. 3970-3987, 2011.

[34] K. Subrahmanyam, S. Vivekchand, A. Govindaraj, C. Rao, A study of graphenes prepared by different methods: characterization, properties and solubilization, *J. Mater. Chem.*, vol. 18, pp. 1517-1523, 2008.

[35] P. Bouvrette, S. Hrapovic, K. B. Male, J. H. Luong, Analysis of the 16 Environmental Protection Agency priority polycyclic aromatic hydrocarbons by high performance liquid chromatography-oxidized diamond film electrodes, *J. Chromatogr. A*, vol. 1103, pp. 248-256, 2006.

[36] J. Costa, A. Sant'Ana, P. Corio, M. Temperini, Chemical analysis of polycyclic aromatic hydrocarbons by surface-enhanced Raman spectroscopy, *Talanta*, vol. 70, pp. 1011-1016, 2006.

[37] C. A. Paddon, C. E. Banks, I. G. Davies, R. G. Compton, Oxidation of anthracene on platinum macro-and micro-electrodes: Sonoelectrochemical, cryoelectrochemical and sonocryoelectrochemical studies, *Ultrason. Sonochem.*, vol. 13, pp. 126-132, 2006.
[38] D. S. Cordeiro, P. Corio, Electrochemical and photocatalytic reactions of polycyclic aromatic hydrocarbons investigated by raman spectroscopy, *J. Braz. Chem. Soc.*, vol. 20, pp. 80-87, 2009.
[39] S. N. Mailu, T. T. Waryo, P. M. Ndangili, F. R. Ngece, A. A. Baleg, P. G. Baker, E. I. Iwuoha, Determination of anthracene on Ag-Au alloy nanoparticles/overoxidized-polypyrrole composite modified glassy carbon electrodes, *Sensors*, vol. 10, pp. 9449-9465, 2010.
[40] N. G. Mathebe, A. Morrin, E. I. Iwuoha, Electrochemistry and scanning electron microscopy of polyaniline/peroxidase-based biosensor, *Talanta*, vol. 64, pp. 115-120, 2004.